Journal of Peptide Science, Vol. 2, 176–193 (1996)

Conformational Analysis of Neuropeptide Y Segments by CD, NMR Spectroscopy and Restrained Molecular Dynamics

MARION GURRATH[1], ALESSANDRO BISELLO[1], KATIA BOTTAZZO[1], CHUN-WA CHUNG[2], STEFANO MAMMI[1] and EVARISTO PEGGION[1]

[1] University of Padua, Biopolymer Research Center, Department of Organic Chemistry, 35131 Padua, Italy
[2] Glaxo Wellcome, Biomolecular Structure Group, Stevenage, UK

Received 13 November 1995
Accepted 15 January 1996

Neuropeptide Y (NPY), a peptide amide comprising 36 residue has been shown to act as a potent vasoconstrictor. In order to shed light on the structural requirements for the biological activities with respect to the different prerequisites for affinity to the NPY receptor subtypes Y_1 and Y_2, in the present study the syntheses and conformational analyses of two C-terminal segments, NPY(18–36) and NPY(13–36), are described.

The results obtained by CD measurements, two-dimensional NMR spectroscopy and a conformational refinement of the NMR-derived structure by molecular mechanics simulations support the findings of previously published structure–activity relationship studies for biologically active and selective compounds. In particular, the α-helical conformation as well as an appropriate exposure of the side chains of the critical C-terminal dipeptide within NPY(18–36) are in agreement with the prerequisites proposed for Y_2 receptor binding of that segment.

Keywords: NPY; conformational analysis (CD, NMR); molecular dynamics

INTRODUCTION

Neuropeptide Y (NPY) is an oligopeptide amide comprising 36 residues, originally isolated from porcine brain [1], which is distributed throughout the central and peripheral nervous system [2, 3]. Co-released with noradrenaline from sympathetic neurones, it has been shown to be involved in the control of the cardiovascular system, acting as a potent long-lasting vasoconstrictor [4].

NPY is a member of related, homologous peptides [5] characterized by a common structural motif which is known as the pancreatic polypeptide fold (PP-fold). This structural feature was first identified for the avian pancreatic polypeptide (APP) by X-ray crystallography [6] and can be described as a polyproline type II helix within the N-terminal part packed against a well-defined α-helix spanning the C-terminal region. Both helices, which are joined by a type II β turn, show an amphiphilic surface. The hydrophobic residues are exposed on the interface area resulting in the interaction of prolines with aromatic side chains of the α-helix through hydrophobic contacts.

The amino acid sequences of the avian pancreatic peptide and human NPY are the following:

APP GPSQP TYPGD DAPVE DLIRF YDNLQ QYLNV VTRHR Y-NH_2

hNPY YPSKP DNPGE DAPAE DMARY YSALR HYINL ITRQR Y-NH_2

The first structural information of human NPY (hNPY) was derived by a molecular modelling study based on the X-ray structure of APP [7–9]. During the past few years several groups have studied NPY and analogues by means of NMR spectroscopy, obtaining

Address for correspondence: Prof. E. Peggion, University of Padua, Biopolymer Research Center, Department of Organic Chemistry, Via Marzolo 1, 35131 Padua, Italy.

CCC 1075-2617/96/030176-18

diverse results which depend mainly on solvent conditions [10–17]. Some structural information on the segment NPY(18–36) was derived from CD spectroscopy studies [18]. This segment has been shown to act as a non-competitive NPY antagonist, lowering blood pressure [18, 19], but the mechanisms of action still remain unsolved. On the other hand, the segment NPY(13–36) competes with NPY for binding sites in rat brain and mimics the inhibitory effects of NPY at presynaptic receptors in rats. However, in its NPY–receptor binding affinities, it is less potent than the native peptide [20–22].

In an attempt to correlate structural characteristics with opposite overall biological activities, the present study describes the elucidation of the conformation in solution of both segments, NPY(18–36) and NPY(13–36), respectively:

pNPY(13–36) PAE DLARY YSALR HYINL ITRQR Y-NH_2

NPY(18–36) ARY YSALR HYINL ITRQR Y-NH_2

MATERIALS AND METHODS

Materials

Fmoc-protected amino acids were obtained from Bachem, while Fmoc-protected amino acids–N-carboxy-anhydride (NCA) were purchased from Propeptide. NMP, DCM, piperidine, HOBt, HBTU, DCC, acetic anhydride and TFA were purchased from Applied Biosystems. DIEA, ethanedithiol, thioanisol and trimethylsilyl bromide were from Fluka. Acetonitrile and phenol were obtained from Carlo Erba.

Instrumentation and Methods

Peptide synthesis was performed by the solid-phase method using an applied Biosystems model 431A automated peptide synthesizer. High-performance liquid chromatography (HPLC) purification was carried out on a Perkin Elmer series 3B chromatography equipped with a Perkin Elmer LC75 UV detector and a Perkin Elmer Sigma 15 data station. The following Waters columns were used: Deltapack C-18 RF 300 Å (3.9 × 300 mm), $\phi = 15$ μm, for analytical runs; Deltapack C-18 RF 100 Å (19 × 300 mm), $\phi = 15$ μm for preparative runs.

Amino acid analyses were carried out on a model Carlo Erba Automatic Amino Acid Analyser interfaced with a Shimadzu C-R4A Chromatopac Recorder.

Capillary electrophoresis runs were carried out on an Applied Biosystem A 270 capillary electrophoresis system.

CD spectra were recorded with a JASCO Model J-600 automatic spectropolarimeter, interfaced with a personal computer. Quartz cells with optical pathlengths of 0.001, 0.01 and 0.1 cm were used.

NMR Measurements. NMR experiments were performed at 308 K on Bruker AM 400 and AMX 600 spectrometers; the derived data were processed on a Bruker X-32 computer with UXNMR software. The concentration of NPY(18–36) was 1.55 mM for DQF-COSY [23] and TOCSY [24] experiments and was increased to 2.33 mM for the acquisition of NOESY [25], P.E.COSY [26] and heteronuclear experiments, i.e. HMQC [27, 28] experiments and HSQC with TOCSY transfer [29, 30]. All these experiments were acquired at 600 MHz in a mixture of TFE-d_2 and H_2O 9:1. The NMR sample of NPY(13–36) contained 2.39 mM peptide in a TFE-d_3/H_2O mixture 9:1, which was used for data acquisition at 400 MHz. All two-dimensional NMR spectra were obtained following the TPPI method [31, 32] with experiments of 2 K data points. Prior to Fourier transformation the time domain data were multiplied by phase-shifted sine-squared, or Gaussian window functions in both dimensions, and zero filling was carried out to 2 K × 1 K real points. The baseline was corrected in both dimensions with a polynomial of degree 3, 4 or 5. For spin lock the DIPSI sequence [33] cycled 4 and 16 times (20–80 ms, 600 MHz) and the MLEV-17 sequence were used, the latter containing delays characteristic of a clean TOCSY [34] cycled 21 times with trim pulses of 2.5 ms, each resulting in a mixing time of 70 ms (400 MHz). Two-dimensional NOESY spectra were recorded with mixing periods of 150 ms. A 5% random variation of the mixing period was applied in order to reduce zero quantum coherence contributions [35]. Homonuclear vicinal coupling constants ($^3J_{HH}$) extracted from P.E.COSY cross peaks were used in combination with characteristic NOEs for the assignment of diastereotopic H^β protons and determination of the ratio of rotamers concerning the orientation of amino acid side chains. NOESY spectra were used for quantitative determination of the strengths of NOE intensities by integrating and calibrating the cross-peak volumes.

The heteronuclear ^1H, ^{13}C correlated spectra were recorded with a spectral width of 6024 Hz in F2 (^1H) and 27,000–38,000 Hz in F1 (^{13}C), a relaxation delay of 1–1.3 s, 128–240 scans, and GARP decoupling were applied [36]. The DIPSI sequence within the HSQC with TOCSY transfer was cycled 8 and 15 times, resulting in mixing periods of 44 and 82.5 ms, respectively.

Computational Methods. The NMR-derived conformational relavant parameters were translated into 3D structure information by application of NOE-restrained molecular dynamics simulations. All model-building procedures, interactive animations, graphical analyses and simulations were carried out using the Insight-II/Discover molecular modelling package (Biosym Technologies Inc., San Diego, CA) [37]. For all energy minimizations (EM) and molecular dynamics (MD) simulations the consistent valence force field as implemented in Version 2.80 of Discover was used without Morse potentials for bond stretching interactions and without cross terms. The equation of motion was integrated numerically by applying the Verlet algorithm with a time step of 1 fs. For all *in vacuo* simulations a dielectric permittivity of 78 was used in order to minimize artificial long-range charge–charge interactions. The starting structure of the linear peptide amide was generated interactively by assuming an ideal α-helix backbone conformation. All amino acid residues were retrieved from the Insight-II residue library together with the force field parameters. In accordance with the results obtained from NMR all peptide bonds were restrained in *trans* configuration throughout all simulations applying an harmonic dihedral forcing potential of $k_\Theta = 10.0$ kcal/mol/rad^2. For the residues Ile^{28}, Asn^{29}, Ile^{31}, Thr^{32} and Arg^{35} the mainly populated side-chain (χ_1) rotamer was identified by combining NOE and homonuclear coupling constant information. Therefore, the affected χ_1 torsion angles were restrained to the corresponding staggered rotamers. The distance restraints finally applied were obtained by imposing a tolerance of $\pm$ 10% (r^{up}, r^{low}) on each distinct interproton distance derived from the NOE cross-peak integration and calibration procedure. This should enable the molecular system to explore an enlarged fraction of the available conformational space during MD simulations, even if distance restraints were applied. Furthermore, a 10% distance tolerance accounts for errors inherently linked to the approximations underlying the calibration of NOE cross peaks, such as two-spin approximation and isotropic motional reorientation.

The starting structure was relaxed over 1000 steps of conjugate gradient minimizations in order to remove conformational strain caused by the model-building procedure. After this relaxation the molecule was initialized at a temperature of 300 K over 1 ps, followed by a 150 ps restrained MD simulation. The initial 50 ps of the total 150 ps trajectory was used to smoothly introduce the NOE-derived distance restraints. For this purpose, the force constant describing the distance restraining penalty function was gradually increased in 10 steps each covering 5 ps, until the final value of $k = 5000$ kcal mol Å^2 was reached. The distance restraining force constant was kept at its final value over the subsequently simulated 100 ps of molecular dynamics. The entire trajectory was updated every 1 ps, yielding an ensemble of 150 distinct conformations. For the purpose of structural analyses the last 50 snapshots were conformationally averaged and minimized over 500 steps of restrained EM applying the conjugate gradients algorithm.

All conformational details described in the Result and Discussion section refer to this final structure.

Peptide Synthesis and Purification

The resin contained Fmoc-4-methoxy-4′-(γ-carboxypropyl)-benzhydrylamine linked to alanyl-aminoethyl-polystyrene/1% divinylbenzene (substitution 0.6 mmol/g) (obtained from Bachem). Side-chain protection of the Fmoc-protected amino acids was as follows: *t*Bu for Tyr, Ser, Asp and Glu; Trt for His, Asn and Gln, and Mtr for Arg. NMP was the solvent for the coupling, and the deprotection was carried out with piperidine 20% in NMP.

NPY(13–36). Fmoc-protected amino acids were activated with HOBt/DCC in NMP. A four-fold excess of activated amino acid was used and an acetylation step with acetic anhydride of the unreacted amino groups was performed after each coupling. The coupling yield was measured with quantitative ninhydrin tests on a small sample of the resin. The peptide was cleaved and deprotected in two steps, owing to the presence of multiple Arg(Mtr) residues. The peptidyl–resin was treated with TFA/thioanisol/phenol/ethanedithiol/water (83:4:6:4:3) at 25 °C for 4 h. After filtration and evaporation of the volatiles the residual Mtr groups were cleaved with TFA/thioanisol/trimethylsilyl bromide (6:1:1) at 0 °C for 1 h. After concentration under reduced pressure water was added and the solution extracted with diethyl ether. The crude peptide was recovered by lyophilization and purified in a single step by reversed phase HPLC with a linear elution gradient of acetonitrile/water from 18% to 42% MeCN over 30 min in the presence of 0.05% TFA. The final product was lyophilized and its purity assessed by analytical HPLC in several eluting systems, and by capillary electrophoresis in 20 mM citrate buffer, pH 2.5. The

amino acid analysis of the acidic hydrolysate yielded the following amino acid ratios: Asp 1.96 (2), Thr 0.96 (2), Ser 1.00 (1), Glu 2.03 (2), Pro 1;00 (1), Ala 2.86 (3), Ile 2.00 (2), Leu 3.03 (3), Tyr 4.10 (4), His 0.96 (1), Arg 4.30 (4). The HPLC and capillary electrophoresis profiles of the purified product are shown in Figure 1.

By fast-atom bombardment mass spectrometry the correct molecular weight of 2982 Da was obtained. The peptide content of the sample, determined by quantitative amino acid analysis, was 75%.

NPY(18–36). Four equivalent of Fmoc–N-carboxyanhydride were used (in the case of Arg(Mtr) and His(Trt) activation with HOBt/DCC was used instead) in NMP. (The different synthetic route was followed within a frame of a research programme addressed to comparing different methodologies to obtain various NPY fragments. The results of these synthetic studies extended to a series of NPY fragments will be reported elsewhere.) The coupling efficiency was measured with quantitative ninhydrin tests and a capping cycle

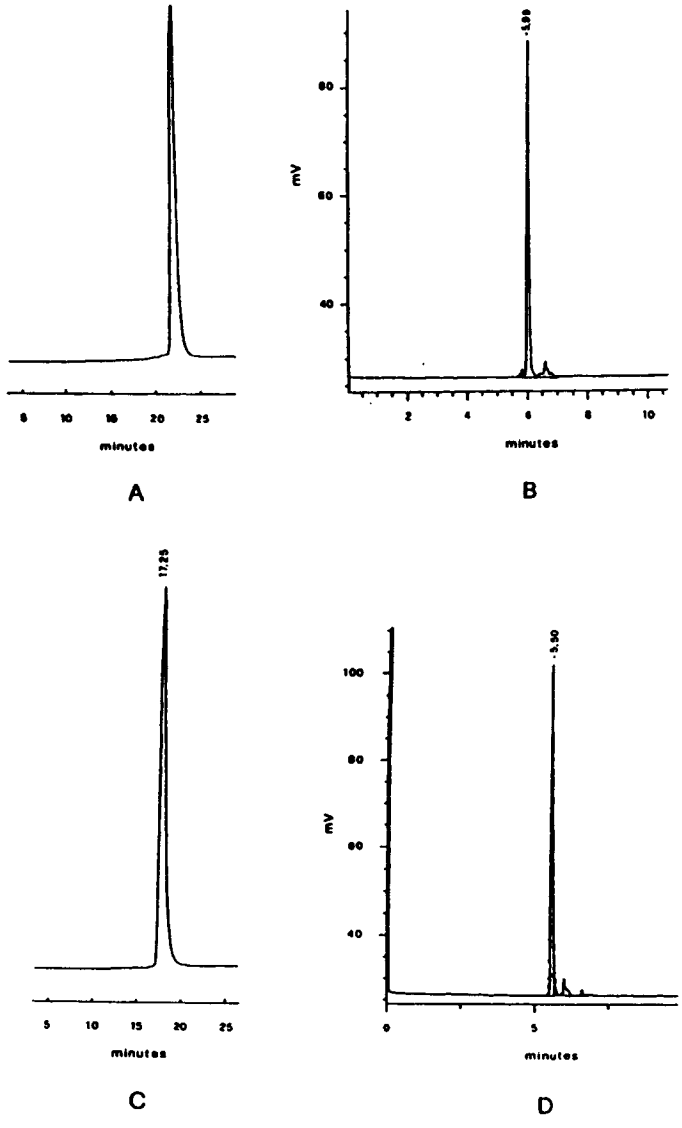

Figure 1 HPLC (A) and capillary electrophoresis (B) profiles of purified NPY(13–36) and NPY(18–36) (C, D). HPLC column Deltapack RP C-18, 300 Å (3.9 × 300 mm), 15 μ. Eluent A: 90% MeCN + 10% water containing 0.05% TFA. Eluent B: 10% MeCN + 90% water containing 0.05% TFA. The capillary electrophoresis run was carried out in 20 mM citrate buffer, pH 2.5.

was added at the end of each coupling. The peptide was cleaved from the resin using TFA/thioanisol/-phenol/ethanedithiol/water (83:4:6:4:3) at 25 °C for 4 h and at 55 °C for 30 min. After filtration and concentration by evaporation under reduced pressure, water was added to the residual oil and the aqueous solution extracted with diethyl ether and lyophilized. A first purification was carried out with a gradient from 18% to 42% MeCN, in the presence of 0.05% TFA, over 30 min. Because of the presence of a small hydrophobic impurity, a second purification was necessary. In this case a linear gradient from 15% to 58% MeCN, in the presence of 43 mM triethylamine and 74 mM phosphoric acid, was used. The purified peptide was then desalted with water-/MeCN gradient from 18% to 34% acetonitrile over 10 min in the presence of 0.05% TFA. The final product was lyophilized and its purity assessed by analytical HPLC in several eluting systems, and by capillary electrophoresis in 20 mM citrate buffer pH 2.5. The amino acid analysis of the acidic hydrolysate yielded the following amino acid ratios: Asp 0.97 (1), Thr 0.92 (1), Ser 0.86 (1), Glu 0.96 (1), Ala 1.87 (2), Ile 1.94 (2), Leu 1.96 (2), Tyr 4.36 (4), His 0.90 (1), Arg 4.38 (4). The HPLC and capillary electrophoresis profiles of the purified product was shown in Figure 1. By fast-atom bombardment mass spectrometry the correct molecular weight of 2456 Da was obtained. The peptide content of the sample, determined by quantitative amino acid analysis, was 74%.

RESULTS

CD Studies

The CD spectrum of the NPY(18–36) segment in aqueous solution is typical of a disordered conformation (Figure 2) and is independent of peptide concentration in the range 2.45×10^{-5} to 2.45×10^{-3}. Addition of increasing amounts of TFE induces helix formation as revealed by the typical CD spectrum with two negative maxima at 222 and 208 nm. The maximum helix content (saturation conditions) is reached in the presence of 30% TFE. Under saturation conditions the helix content estimated from the amplitude of the negative band at 222 nm is ≈65%. Helix formation is also induced by addition of SDS to an aqueous peptide solution. In this case the maximum helix content, reached in the presence of 17.6 mM SDS, is of ≈55%, i.e. lower than in TFE (data not shown).

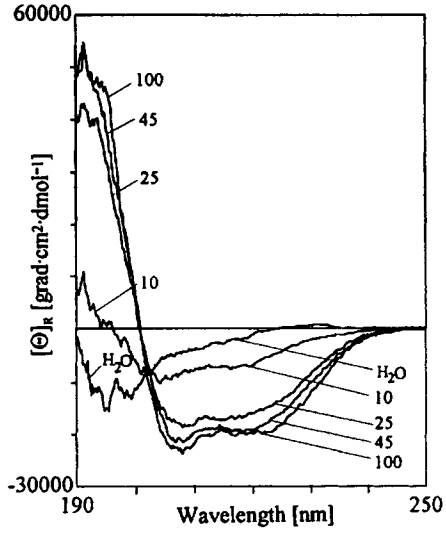

Figure 2 CD spectra of NPY(18–36) segment in water/TFE mixtures. TFE percentages are indicated on the spectra.

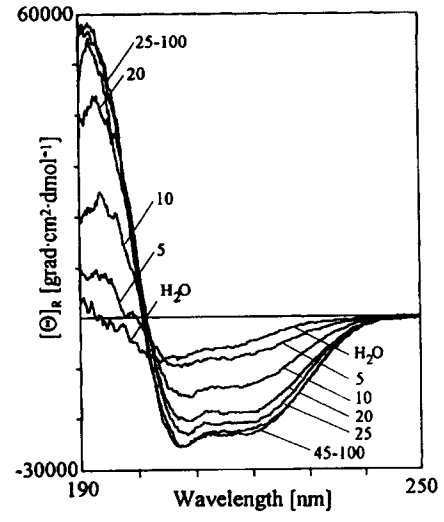

Figure 3 CD spectra of NPY(13–36) segment in water/TFE mixtures. TFE percentages (v/v) are indicated on the spectra.

The results of CD measurements on the NPY segment (13–36) are shown in Figure 3. In this case the conformation in aqueous solution appears to be more ordered than that of the shorter segment. In fact there is an evident shoulder around 220 nm and a negative maximum around 205 nm. Again, increasing amounts of TFE induce the presence of the α-helical structure, with a maximum helix content of ≈80%, reached in the presence of 30% TFE (v/v). In the presence of SDS the maximum helix content, reached in 17.7 mM detergent, is of ≈65% (data not shown).

NMR Studies

NPY(18–36). Spectra of the segment NPY(18–36) in a 9:1 TFE/H_2O mixture showed a single set of resonances, indicating that the molecule adopts a single conformation within the NMR time scale. Especially in the NH region, lines are broad, owing to the viscosity of the solution as reported for hNPY in a TFE/H_2O mixture [13].

The peptide contains several identical amino acids leading to the same spin systems. The DQF-COSY spectrum is well separated concerning resonances of 12 amino acids. However, both $Leu^{24/30}$NH protons show nearly the same chemical shift (Table 1). While Arg^{19} and Arg^{25} are well separated from Arg^{33} and Arg^{35}, the latter overlap in both the F2 and the F1 directions and their resonances are nearly identical to that of Ala^{23}. Also the NH protons of His^{26} and Thr^{32} are isochrone and their chemical shift values are found to be almost the same as Glu^{34}NH. One of the main problems turned out to be the assignment of protons belonging to the aliphatic side chains of isoleucine and leucine, both representing an A_3B_3MPT spin system [38]. Within these spin systems an overlay of LeuH^{β} protons and LeuH^{γ} protons, and also of, for example, $Ile^{31}H^{\beta}$ with $Ile^{28}H^{\gamma}$ could be observed (Table 1), rendering it difficult to achieve an unambiguous assignment. The details of the TOCSY spectrum (Figure 4) containing correlations within the aliphatic region allowed us to solve these problems. The $Ile^{31}\delta CH_3$ (0.78 p.p.m.) resonance is high-field shifted. Therefore, this chemical shift value could serve as a probe for all other resonances belonging to the Ile^{31} spin system (Table 1). Using the TOCSY spectrum shown in Figure 4, all proton resonances of isoleucine and leucine side-chains could be assigned.

Chemical shift values were verified by taking ^1H, ^{13}C correlations into account. For this purpose an HMQC experiment was recorded to detect direct connectivities (Figure 5) whereas the HSQC with TOCSY transfer shows long-range correlations, needed for unambiguous assignment. The ^{13}C chemical shift resonances are shown in Table 2. Because of the larger dispersion within the carbon dimension (F1) it is possible to assign amino acids with identical proton resonances (F2). The detail of the HMQC spectrum in Figure 5 shows direct ^1H, ^{13}C connectivities within the aliphatic region. The HMQC experiment, for example, allowed the dispersion of $Ile^{28}H^{\gamma}$ and $Ile^{31}H^{\beta}$ displaying the same ^1H chemical shift

Table 1 ^1H Assignment of $NPY_{(18-36)}$[a]

Residue	NH	H^{α}	H^{β}	$H^{\beta\prime}$	H^{γ}	$H^{\gamma\prime}$	H^{δ}	$H^{d\prime}$	Others
Ala^{18}	–	4.17	1.57 CH_3^{β}	–	–	–	–	–	
Arg^{19}	8.48	4.36	1.83		1.68		3.25		NH^{ε} 7.05
Tyr^{20}	7.75	4.50	3.15/3.10		–	–	–	–	2,6-H 7.06; 3,5-H 6.68
Tyr^{21}	7.53	4.40	~3.15		–	–	–	–	2,6-H 7.13; 3,5-H 6.91
Ser^{22}	7.86	4.28	4.08	4.03	–	–	–	–	OH–
Ala^{23}	7.94	4.26	1.61 CH_3^{β}	–	–	–	–	–	
Leu^{24}	7.99	4.31	1.88	1.76	1.78	–	1.11 CH_3^{δ}	1.05 $CH_3^{\delta\prime}$	–
Arg^{25}	8.17	4.04	1.94		1.75	1.66	3.22		NH^{ε} 7.12
His^{26}	8.11	4.46	3.47		–	–	–	–	2-H 8.45; 4-H 7.23
Tyr^{27}	8.36	4.35	~3.35		–	–	–	–	2,6-H 7.15; 3,5-H 6.84
Ile^{28}	8.71	3.78	2.03	1.02 CH_3^{γ}	1.92	1.42	0.95 CH_3^{δ}	–	–
Asn^{29}	8.21	4.42	3.12	2.88	–	–	–	–	$CONH_2$ 7.44, 6.38
Leu^{30}	8.00	4.15	1.85		1.70	–	0.94 $CH_3^{\delta 2}$		–
Ile^{31}	8.41	3.91	1.92	0.89 CH_3^{γ}	1.47	1.24	0.78 CH_2^{δ}	–	–
Thr^{32}	8.11	4.10	4.46	–	1.42 CH_3^{γ}	–	–	–	OH–
Arg^{33}	7.95	4.23	2.08		1.89	1.84	3.26		NH^{ε} 7,10
Gln^{34}	8.13	4.18	2.25		2.57	2.47	–	–	$CONH_2$ 6.91, 6.20
Arg^{35}	7.95	4.21	1.80	1.72	1.48		3.12		NH^{ε} 6.88
Tyr^{36}	7.81	4.68	3.32	2.98	–	–	–	–	2,6-H 7.26; 3,5-H 6.85; $CONH_2$ 7.21, 6.50

[a] 1.55 mM $NPY_{(18-36)}$ in 0.5 ml TFE-d_2/H_2O 9:1 at T = 308 K. Chemical shift values are referenced to TFE (3.94 p.p.m.).

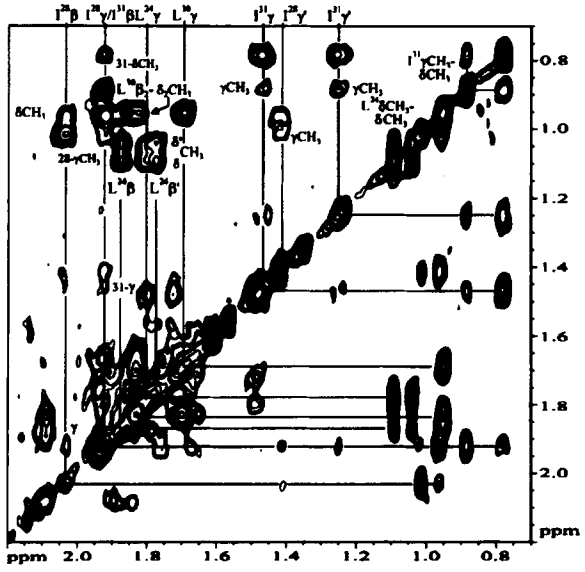

Figure 4 Aliphatic region of a 70 ms TOCSY spectrum of NPY(18–36). The Ile and Leu spin systems are indicated.

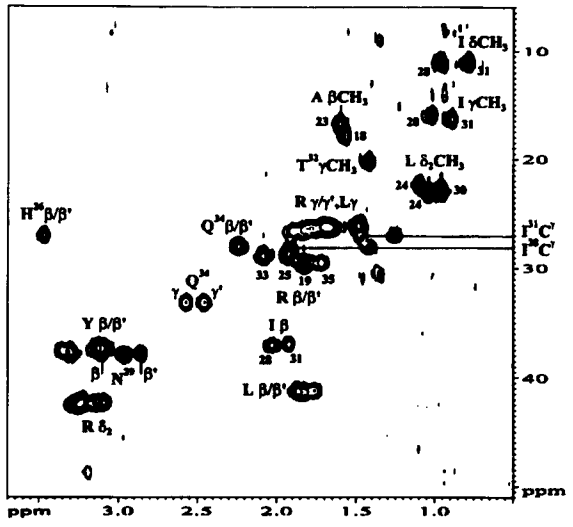

Figure 5 Aliphatic region of a HMQC spectrum of NPY(18–36).

(Table 1) in the ^{13}C dimension because $Ile^{28}C^{\gamma}$ (28.1 p.p.m.) and $Ile^{31}C^{\beta}$ (37.0 p.p.m.) resonances are widely separated. Also the chemical shift values of $H^{\beta\prime}$ (1.76 p.p.m.) and H^{γ} (1.78 p.p.m.) of Leu^{24} could be assigned correctly from C^{β} (41.4 p.p.m.) and C^{γ} (26 p.p.m.) resonances in F1. A further illustrative example is given by the assignment of the δ-methyl groups of Ile^{28} and Leu^{30}, respectively. $Ile^{28}\delta CH_3$ and $Leu^{30}\delta_2CH_3$ turned out to be isochrone in the F2 dimension (Table 1), whereas the ^{13}C chemical shift values are well separated ($Ile^{28}\delta CH_3$: 11.0 p.p.m., $Leu^{30}\delta_2CH_3$: 23.0 p.p.m.).

From the NH–NH region of the NOESY spectrum (Figure 6) almost all possible sequential NH–NH correlations are observable, from which the sequen-

Table 2 ^{13}C Assignment of $NPY_{(18-36)}$[a]

Residue	C^{α}	C^{β}	C^{γ}	C^{δ}	Others
Ala^{18}	51.6	18.0 CH_3^{β}	–	–	–
Arg^{19}	56.8	30.0	26.3	42.6	–
Tyr^{20}	58.9	37.5	–	–	3,5-C 117.5; 2,6-C 132.4
Tyr^{21}	59.6	37.5	–	–	3,5-C 118.0; 2,6-C 132.4
Ser^{22}	60.5	62.6	–	–	–
Ala^{23}	54.8	16.8 CH_3^{β}	–	–	–
Leu^{24}	57.8	41.4	~26	22.2 CH_3^{δ}, 23.0 $CH_3^{\delta\prime}$	
Arg^{25}	58.5	28.8	~26	42.6	–
His^{26}	58.9	27.0	–	–	2-C 135.0; 4-C 119.5
Tyr^{27}	61.0	37.8	–	–	3,5-C 117.5; 2,6-C 132.4
Ile^{28}	64.0	37.1	28.1	16.0 CH_3^{γ}	11.0 CH_3^{δ}
Asn^{29}	56.2	37.9	–	–	$CONH_2$
Leu^{30}	58.0	41.4	~26	23.0 $CH_3^{\delta 2}$	–
Ile^{31}	63.6	37.0	27.1	16.4 CH_3^{γ}	11.0 CH_3^{δ}
Thr^{32}	65.3	68.8	20.2 CH_3^{γ}	–	–
Arg^{33}	57.5	29.0	26.8	42.6	–
Gln^{34}	56.8	28.1	33.5	–	$CONH_2$
Arg^{35}	57.5	30.0	26.0	42.6	–
Tyr^{36}	71.2	38.0	–	–	3,5-C 117.5; 2,6-C 132.6

[a] 2.33 mM $NPY_{(18-36)}$ in 0.4 ml TFE-d_2/H_2O 0:1, at T=308 K.
The ^{13}C chemical shift values are referenced to TFE (61.5 p.p.m.).

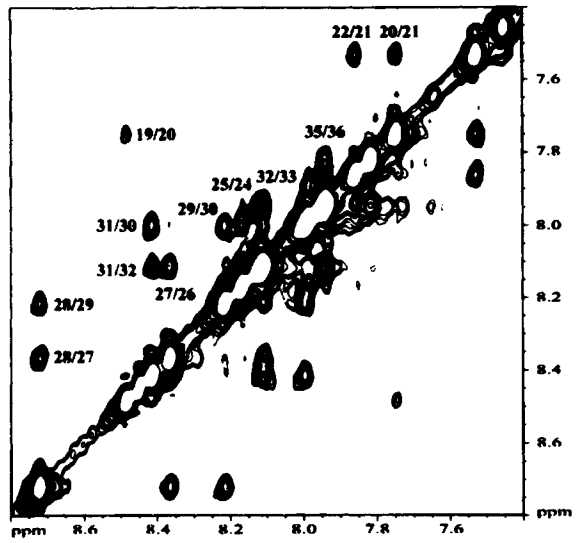

Figure 6 NH-NH correlations within a 150 ms NOESY spectrum of NPY(18–36).

tial assignment emerges. The sequential stretches Ser^{22}-Ala^{23}-Leu^{24} and Arg^{25}-His^{26} and Arg^{33}-Glu^{34}-Arg^{35}-Tyr^{36} cannot be sequenced unambiguously because of close proximity of the cross peaks to the diagonal or mutual NH resonance overlap, e.g. Arg^{33}NH and Arg^{35}NH (7.95 p.p.m.). Nevertheless, 12 out of 18 theoretically possible sequential inter-residue NH–NH correlations are assignable. The analysis of the NOESY fingerprint region allowed us to complete the sequential assignment. After volume integration and calibration the NOEs were categorized in three classes, strong (1.8–2.5 Å), medium (1.8–3.5 Å) and weak (1.8–5.0 Å), yielding the NOE pattern shown in Table 3. The NOEs of the type NH(i)-NH($i+1$) are quite indicative for an α-helical folding. However, stronger evidence for an α-helix is given by correlations following an i to $i+3$ pattern (H^{α}-NH, H^{α}-H^{β}). Based on the NOEs, the α-helical folding of NPY(18–36) comprises at least residues 19–33 but not excluding the extension in the C-terminal direction (Table 3).

Special emphasis should be laid on the obvious gap stretching from Ser^{22} to Arg^{25} within the four lanes which describe i to $i+1$ correlations. It should be stressed that this gap results from signal overlap and is *not* due to missing spatial connectivities. The gap is clearly closed by taking into account $H^{\alpha}(i)$-$H^{\beta}(i+3)$ medium-range correlations indicating a continuous helical stretch. A comparable observation is made within the C-terminal part (Table 3).

The structural motif of an α-helix is also confirmed by a negative deviation of the H^{α} resonances of the segment, compared to the chemical shift values in a random structure [39]. Tyr^{36} is the only exception with a slighly positive H^{α} deviation.

A further structural relevant parameter, i.e. the homonuclear vicinal coupling constant $^3J_{HH}$ was extracted from a P.E.COSY spectrum. Comparative analysis of intra-residue H^{α}-H^{β} and NH-H^{β} NOEs, and $H^{\alpha}H^{\beta}$ coupling constants, allowed the diastereotopic assignment of Ser^{22}, Asn^{29}, Arg^{35} and Tyr^{36}. Calculation of the major populated side-chain rotamer according to Pachler [40] resulted for five amino acids (Ile^{28}, Asn^{29}, Ile^{31}, Thr^{32}, Arg^{35}) in a more than 50% populated staggered low-energy conformation regarding χ_1 (Table 4). Since these side-chain populations exceed the 50% threshold, the corresponding dihedral angles served as NMR-derived restraints in the performed molecular mechanics simulations.

NPY(13–36). The N-terminal elongated segment NPY(13–36) was studied by NMR under the same experimental conditions as the NPY(18–36) segment. Close inspection of the fingerpring region of a DQF–COSY spectrum reveals severe NH resonance overlap. For residues His^{26} and Asn^{29} not only are the NH resonances identical, but the H^{α} resonances of both residues also display the same chemical shift values (Table 5).

The 70 ms TOCSY spectrum (Figure 7) clearly shows that the corresponding COSY cross peaks account for both the His^{26} and Asn^{29} NH-H^{α} correlations, since the H^{β} resonances of more than a single amino acid are found at the NH trace at $\delta = 8.18$ p.p.m. The final assignment for these two residues was only possible with assistance of sequential inter-residue correlations extracted from a NOESY spectrum.

Other overlapping COSY peaks were observed for Ala^{14}, Glu^{15} and Tyr^{27}, for Ala^{18}, Arg^{19} and Arg^{33}, Arg^{35}, and also Arg^{25} and Ile^{31}. In fact, an observed NOE is certainly composed of more than one inter-proton correlation, all contributing to the cross-peak intensity. The qualitative NOE pattern was extracted from a 150 ms NOESY spectrum. The majority of the expected NOESY cross peaks indicating close spatial proximities cannot be determined unambiguously, thus preventing a quantification in terms of inter-porton distances. As a consequence, a quantitative conformational anlaysis by means of restrained molecular mechanics simulations could not be performed, since the number of usable restraints is far too low for a meaningful description of the peptide conformation.

Table 3 Summary of NOEs of $NPY_{(18-36)}$[a]

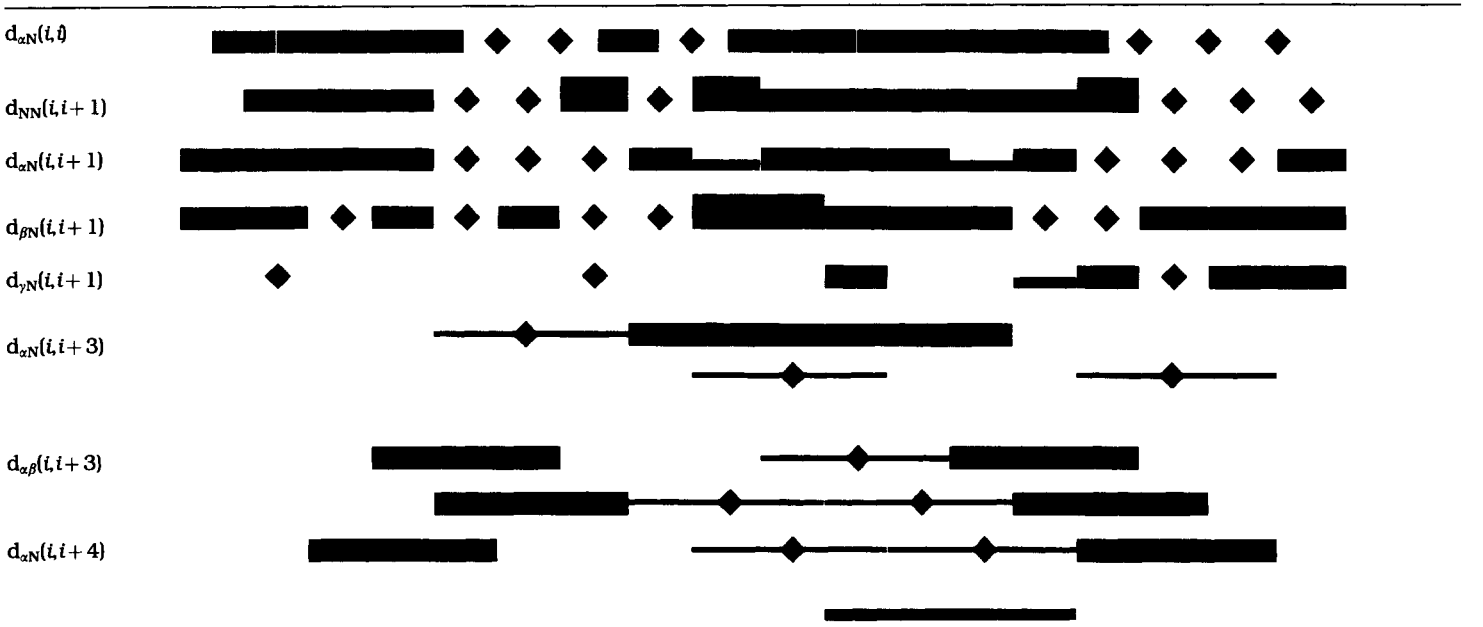

[a] NOE correlations for $NPY_{(18-36)}$ (2.33 mM) in TFE-d_2/H_2O 9:1 at $T = 308$ K.
▬ 1
◆ 1

Table 4 Population of the Major Conformer of Selected Amino Acids of $NPY_{(18-36)}$[a]

Residue	χ_1	Population (%)	Diastereotopic assignment
Ile^{28}	− 60°	95	Defined
Asn^{29}	− 60°	56	H^{β}-*proR*
Ile^{31}	− 60°	86	Defined
Thr^{32}	− 60°	100	Defined
Arg^{35}	− 60°	59	H^{β}-*proR*

[a] The calculation of the side-chain rotamers was performed according to Pachler [40].

Molecular Dynamics of NPY(18–36)

For the reasons explained above, further 3D structural studies were carried out on the segment NPY(18–36) only. The computer-aided conformational analysis of NPY(18–36) is mainly based on interproton distances derived from a NOESY experiment at 600 MHz with a mixing time of 150 ms. Cross-peak intensities provided interproton distances after volume integration and calibration applying the isolated two-spin approximation [41]. For the NPY(18–36) analogue 116 NOE-derived distance restraints served as input data for the restrained molecular mechanics simulations (Table 6).

The conformation of NPY(18–36) obtained after averaging over the last 50 ps of the generated trajectory followed by energy minimization served for the subsequent structural analysis, and will be termed as NPY_AV_EM in the following. The average restraint violation of NPY_AV_EM was found to be 10.6 pm. In total, 55 out of the 116 NOE-derived distance restraints violate the applied potential-free distance range. A violation exceeding 10 pm is analysed for 38 distance restraints; while 15 distance restraints are found outside a 25 pm threshold; only 5 are outside a 50 pm boundary.

The backbone conformation of NPY_AV_EM is characterized by a regular right-handed α-helix

Table 5 ^1H Assignment of $NPY_{(13-36)}$[a]

Residue	NH	H^{α}	H^{β}	$H^{\beta\prime}$	H^{γ}	$H^{\gamma\prime}$	H^{δ}	$H^{\delta\prime}$	Others
Pro^{13}	–	4.45	2.66	2.31	2.23		3.65	3.45	–
Ala^{14}	8.54	4.32	1.58 CH_3^{β}	–	–	–	–	–	–
Glu^{15}	8.50	4.27	2.17		2.62		–	–	OH^{δ}
Asp^{16}	7.97	4.63	2.99		–	–	–	–	OH^{γ} -
Leu^{17}	7.60	4.33	1.93	1.82	–	1.10 CH_3^{δ}	1.00 $CH_3^{\delta\prime}$	–	
Ala^{18}	7.91	4.29	1.62 CH_3^{β}	–	–	–	–	–	–
Arg^{19}	7.89	4.14	2.06		1.90	1.75	3.29		NH^{ε} 7.03
Tyr^{20}	7.92	4.40	3.24		–	–	–	–	2,6-H 7.00; 3,5-H 6.80
Tyr^{21}	8.74	4.33	3.22		–	–	–	–	2,6-H 7.23; 3,5-H 6.92
Ser^{22}	8.27	4.25	4.11		–	–	–	–	OH^{β} -
Ala^{23}	8.21	4.24	1.65 CH_3^{β}	–	–	–	–	–	–
Leu^{24}	8.40	4.24	1.84	1.66	1.66	–		1.00 $CH_3^{\delta 2}$	–
Arg^{25}	8.43	4.01	1.93		1.77	1.60	3.19		NH^{ε} 7.07
His^{26}	8.18	4.42	3.50		–	–	–	–	2-H 8.45; 4-H 7.28
Tyr^{27}	8.53	4.37	3.36		–	–	–	–	2,6H 7.16; 3,5-H 6.84
Ile^{28}	8.84	3.77	2.03	1.03 CH_3^{γ}	1.93	1.41	0.96 CH_3^{δ}	–	–
Asn^{29}	8.18	4.42	3.10	2.85	–	–	–	–	NH_2^{γ} 7.43; 6.35
Leu^{30}	8.03	4.16	1.85		1.71	–		0.98 $CH_3^{\delta 2}$	–
Ile^{31}	8.42	3.93	1.92	0.89 CH_3^{γ}	1.46	1.26	0.78 CH_3^{δ}	–	–
Thr^{32}	8.10	4.10	4.46	1.44 CH_3^{γ}	–	–	–	–	OH^{β} -
Arg^{33}	7.95	4.23	2.10		1.89	1.75	3.27		NH^{ε} 7.09
Gln^{34}	8.13	4.18	2.25		2.58	2.47	–	–	NH_2^{δ} 6.88; 6.15
Arg^{35}	7.92	4.20	1.80	1.74	1.50			3.11	NH^{ε} 6.85
Tyr^{36}	7.81	4.70	3.32	2.96	–	–	–	–	2,6-H 7.28; 3,5-H 6.86
									$CONH_2$ 7.22; 6.43

[a] 2.39 mM $NPY_{(13-36)}$ in TFE-d_3/H_2O (9:1) at T = 308 K.
Chemical shift values are referenced to TFE (3.94 p.p.m.)

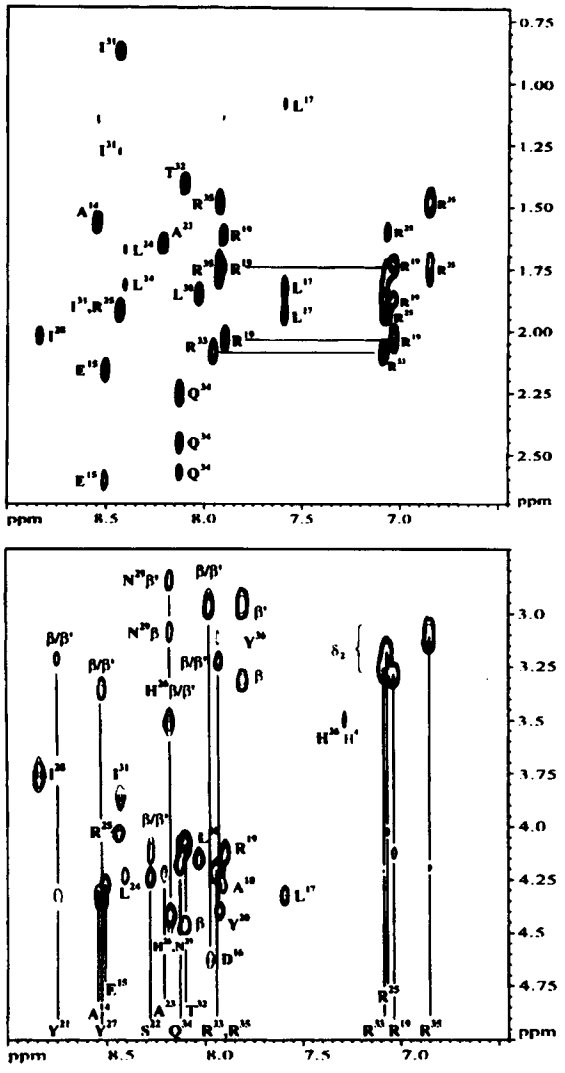

Figure 7 NH trace within the aliphatic region of a 70 ms TOCSY spectrum of NPY(13–36) (above) and the fingerprint region within the same spectrum (below).

comprising residues (Tyr^{21}-Arg^{35}) according to the ideal values for ϕ and ψ of $-57° \pm 20°$ and $-47° \pm 20°$ [42], respectively (Table 7). Obviously the N- and C-terminal residues (Ala^{18}-Tyr^{20}, Tyr^{36}) prefer a somewhat more extended conformation, resulting from averaging over conformations which show increased flexibility in this part. The repetitive hydrogen-bond pattern $C=O^{i} \cdots HN^{i+4}$ is shown in Figure 8.

As a more comprehensive structural analysis we investigated the conformational conservation of the observed α-helix over the course of the MD simulation. In Figure 9 the superposition of 10 snapshots taken in equidistant timesteps of 1 ps from the range

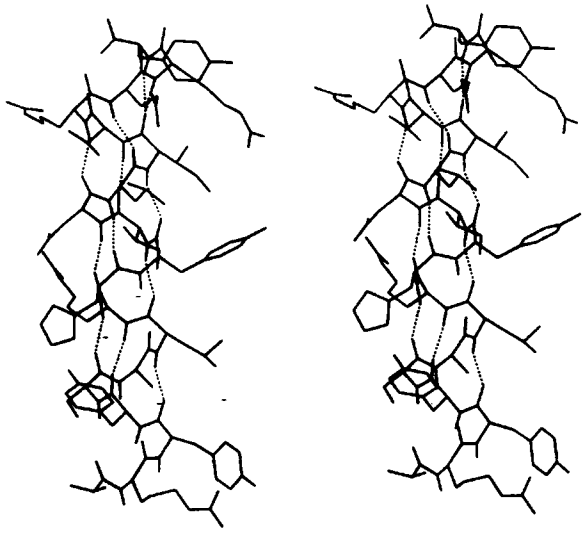

Figure 8 Stereoplot of the minimized conformation of NPY(18–36) obtained after averaging over the last 50 ps of the trajectory. Hydrogen bonds are indicated as dotted lines. The molecule is oriented from the N-terminal (bottom) to the C-terminal (top).

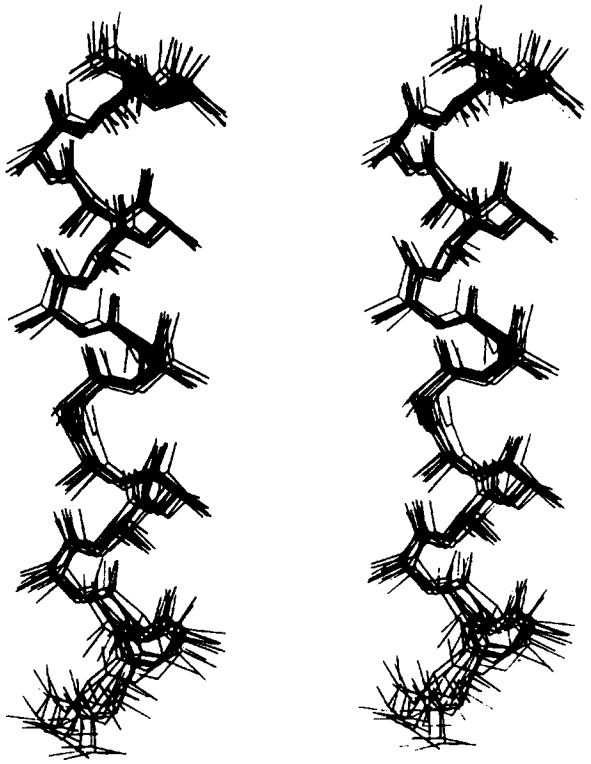

Figure 9 Stereoview of a superposition of 10 snapshots corresponding to structures from 100 to 110 ps of the trajectory. The molecule is oriented from the N-terminal (bottom) to the C-terminal (top); only backbone and C^{β} atoms are indicated.

Table 6 Comparison of NOE-derived Distance Restraints with Corresponding Distances after Structure Refinement[a]

Atom *i*	Atom *j*	r^{up}	r^{low}	NPY_AV_EM	Violation	Atom *i*	Atom *j*	r^{up}	r^{low}	NPY_AV_EM	Violation
$Ile^{28}NH$	$Tyr^{27}NH$	278	227	266	–	$Tyr^{2}NH$	$Tyr^{20}H^{\alpha}$	360	260	349	–
$Ile^{28}NH$	$Asn^{29}NH$	281	230	285	4	$Tyr^{21}NH$	$Tyr^{21}H^{\alpha}$	285	234	298	13
$Ile^{28}NH$	$His^{26}NH$	451	369	435	–	$Ile^{28}NH$	$Ile^{28}H^{\beta}$	249	204	243	–
$Ile^{28}NH$	$Leu^{30}NH$	468	383	411	–	$Ile^{28}NH$	$Ile^{28}CH_3{}^{\gamma}$	434	274	456	22
$Arg^{19}NH$	$Tyr^{20}NH$	338	277	288	–	$Ile^{28}NH$	$Ile^{28}CH_3{}^{\delta}$	460	294	431	–
$Ile^{31}NH$	$Thr^{32}NH$	277	227	284	7	$Arg^{19}NH$	$Arg^{19}H_2{}^{\beta}$	387	243	225	18
$Ile^{31}NH$	$Leu^{30}NH$	277	226	283	6	$Arg^{19}NH$	$Ala^{18}CH_3{}^{\beta}$	335	274	343	–
$Tyr^{27}NH$	$His^{26}NH$	272	223	283	11	$Ile^{3}NH$	$Ile^{31}H^{\beta}$	266	218	244	–
$Tyr^{27}NH$	$Leu^{30}NH$	400	330	457	57	$Ile^{31}NH$	$Leu^{30}H_2{}^{\beta}$	369	228	329	–
$Arg^{33}NH$	$Ile^{31}NH$	425	348	434	8	$Ile^{31}NH$	$He^{31}CH_3{}^{\gamma}$	407	251	457	50
$Asn^{29}NH$	$Leu^{30}NH$	277	227	287	10	$Ile^{31}NH$	$Ile^{31}CH_3{}^{\delta}$	462	296	431	–
$Leu^{24}NH$	$Arg^{25}NH$	270	221	268	–	$Asn^{29}NH$	$Jle^{28}H^{\beta}$	283	232	280	–
$Thr^{32}NH$	$Arg^{33}NH$	250	210	292	42	$Asn^{29}NH$	$Ile^{28}CH_3{}^{\gamma}$	433	273	413	–
$Asn^{29}NH$	$Asn^{29}NH_2$	488	326	426	–	$Arg^{25}NH$	$Arg^{25}H_2{}^{\beta}$	324	191	242	–
$Ser^{22}NH$	$Tyr^{21}NH$	286	243	275	–	$Gln^{34}NH$	$Gln^{34}H_2{}^{\beta}$	343	207	242	–
$Tyr^{20}NH$	$Tyr^{2}NH$	288	236	253	–	$Gln^{34}NH$	$Arg^{33}H_2{}^{\beta}$	381	238	330	–
$Tyr^{36}NH$	$^{37}NH_2$	454	298	432	–	$Thr^{32}NH$	$Ile^{28}CH_3{}^{\gamma}$	565	381	513	–
$Ile^{28}NH$	$Tyr^{27}H^{\alpha}$	334	273	356	22	$Thr^{32}NH$	$Ile^{31}CH_3{}^{\gamma}$	460	294	410	–
$Ile^{28}NH$	$Arg^{25}H^{\alpha}$	334	274	328	–	$Leu^{24}NH$	$Ala^{23}CH_3{}^{\beta}$	375	325	332	–
$Ile^{28}NH$	$Ile^{28}H^{\alpha}$	280	229	296	16	$Arg^{35}NH$	$Gln^{34}H_2{}^{\beta}$	387	243	319	–
$Ile^{28}NH$	$Tyr^{27}H_2{}^{\beta}$	360	221	322	–	$Arg^{33}NH$	$Arg^{33}H_2{}^{\beta}$	335	200	235	–
$Arg^{19}NH$	$Arg^{19}H^{\alpha}$	322	264	292	–	$Ala^{23}NH$	$Ala^{23}CH_3{}^{\beta}$	347	202	278	–
$Arg^{19}NH$	$Ala^{18}H^{\alpha}$	285	233	212	11	$Arg^{35}NH$	$Arg^{35}H_2{}^{\beta}$	402	255	338	–
$Ile^{31}NH$	$Leu^{30}H^{\alpha}$	386	316	357	–	$Arg^{33}NH$	$Thr^{32}CH_3{}^{\gamma}$	437	276	441	4
$Ile^{31}NH$	$Ile^{31}H^{\alpha}$	278	227	295	17	$Ser^{22}NH$	$Ala^{23}CH_3{}^{\beta}$	530	480	535	5
$Ile^{31}NH$	$Ile^{28}H^{\alpha}$	328	268	335	7	$Tyr^{36}NH$	$Arg^{35}H_2{}^{\beta}$	461	303	473	12
$Tyr^{27}NH$	$Tyr^{27}H^{\alpha}$	278	227	297	19	$Tyr^{20}NH$	$Arg^{19}H_2{}^{\beta}$	403	256	356	–
$Tyr^{27}NH$	$Arg^{25}H^{\alpha}$	421	345	423	2	$Tyr^{20}NH$	$Ala^{18}CH_3{}^{\beta}$	390	338	398	8
$Tyr^{27}NH$	$His^{26}H_2{}^{\beta}$	364	224	320	–	$Tyr^{21}NH$	$Arg^{19}H_2{}^{\beta}$	498	334	555	57
$Tyr^{27}NH$	$Tyr^{27}H_2{}^{\beta}$	324	191	228	–	$Tyr^{21}NH$	$Ala^{18}CH_3{}^{\beta}$	502	329	323	6
$Tyr^{27}NH$	$His^{26}H^{\alpha}$	401	328	354	–	$Thr^{32}H^{\beta}$	$Thr^{32}H^{\beta}$	297	243	309	12
$Asn^{29}NH$	$Asn^{29}H^{\alpha}$	343	281	294	–	$His^{26}H^{\alpha}$	$His^{26}H_2{}^{\beta}$	350	213	270	–
$Asn^{29}NH$	$Ile^{28}H^{\alpha}$	366	300	360	–	$Tyr^{21}H^{\alpha}$	$Tyr^{21}H_2{}^{\beta}$	332	198	269	–
$Arg^{25}NH$	$His^{26}H_2{}^{\beta}$	480	319	555	76	$Leu^{24}H^{\alpha}$	$His^{26}H_2{}^{\beta}$	510	335	565	55
$Arg^{25}NH$	$Arg^{25}H_2{}^{\delta}$	492	329	473	–	$Tyr^{27}H^{\alpha}$	$Tyr^{27}H_2{}^{\beta}$	315	184	272	–
$Thr^{32}NH$	$Ile^{31}H^{\alpha}$	315	258	358	43	$Ser^{22}H^{\alpha}$	$Ser^{22}H_2{}^{\beta}$	338	203	230	–
$Thr^{32}NH$	$Ile^{28}H^{\alpha}$	375	307	389	14	$Ala^{23}H^{\alpha}$	$His^{26}H_2{}^{\beta}$	365	225	385	20
$His^{26}NH$	$His^{26}H_2{}^{\beta}$	330	197	308	–	$Arg^{33}H^{\alpha}$	$Arg^{33}H_2{}^{\delta}$	417	267	428	11
$Leu^{30}NH$	$Ile^{28}H^{\alpha}$	397	325	440	43	$Arg^{25}H^{\alpha}$	$Arg^{25}H_2{}^{\delta}$	402	255	277	–
$Leu^{30}NH$	$His^{26}H_2{}^{\beta}$	482	320	529	47	$Arg^{35}H^{\alpha}$	$Arg^{35}H_2{}^{\delta}$	420	270	445	25
$Ser^{22}NH$	$Tyr^{21}H_2{}^{\beta}$	386	242	319	–	$Tyr^{20}H^{\alpha}$	$Ala^{23}CH_3{}^{\beta}$	340	272	340	–
$Tyr^{20}NH$	$Tyr^{20}H_2{}^{\beta}$	347	210	310	–	$Asn^{29}H^{\alpha}$	$Ile^{28}CH_3{}^{\gamma}$	463	297	482	19
$Tyr^{21}NH$	$Tyr^{21}H_2{}^{\beta}$	327	194	245	–	$Leu^{24}H^{\alpha}$	$Ala^{23}CH_3{}^{\beta}$	484	314	509	25
$Arg^{25}NH^{\epsilon}$	$Arg^{25}H^{\alpha}$	404	331	415	11	$Arg^{35}H^{\alpha}$	$Arg^{35}H_2{}^{\beta}$	404	257	258	–
$Arg^{25}NH$	$Arg^{25}H^{\alpha}$	274	224	297	22	$Gln^{34}H^{\alpha}$	$Gln^{34}H_2{}^{\beta}$	343	206	269	–
$Thr^{32}NH$	$Thr^{32}H^{\alpha}$	289	236	291	2	$Arg^{33}H^{\alpha}$	$Arg^{33}H_2{}^{\beta}$	338	203	269	–
$His^{26}NH$	$Arg^{25}H^{\alpha}$	354	290	356	2	$Leu^{30}H^{\alpha}$	$Arg^{33}H_2{}^{\beta}$	378	236	368	–
$Leu^{30}NH$	$Leu^{30}H^{\alpha}$	275	225	295	20	$Ile^{3}H^{\alpha}$	$Gln^{34}H_2{}^{\beta}$	398	252	420	22
$Ser^{22}NH$	$Tyr^{21}H^{\alpha}$	312	255	357	45	$Ile^{31}H^{\alpha}$	$Ile^{31}H^{\beta}$	283	232	306	23
$Ser^{22}NH$	$Ser^{22}H^{\alpha}$	288	235	297	9	$Ile^{31}H^{\alpha}$	$Ile^{31}CH_3{}^{\gamma}$	378	228	325	–
$Tyr^{36}NH$	$Arg^{35}H^{\alpha}$	335	275	357	22	$Ile^{31}H^{\alpha}$	$Ile^{31}CH_3{}^{\delta}$	440	278	465	25

Table 6 (*continued*)

Atom *i*	Atom *j*	r^{up}	r^{low}	NPY_AV_EM	Violation	Atom *i*	Atom *j*	r^{up}	r^{low}	NPY_AV_EM	Violation
$Tyr^{36}NH$	$Thr^{32}H^{\alpha}$	428	350	357	–	$Thr^{32}H^{\alpha}$	$Ile^{32}H^{\alpha}$	482	312	475	–
$Tyr^{20}NH$	$Tyr^{20}H^{\alpha}$	302	245	304	2	$Ile^{28}H^{\alpha}$	$Ile^{28}H^{\beta}$	298	244	8	
$Tyr^{20}NH$	$Arg^{19}H^{\alpha}$	279	228	357	78	$Ile^{28}H^{\alpha}$	$Ile^{28}CH_3^{\gamma}$	379	228	324	–
$Ile^{28}H^{\alpha}$	$Ile^{28}CH_3^{\delta}$	429	269	466	37	$Ala^{18}H^{\alpha}$	$Ala^{18}CH_3^{\beta}$	377	227	254	–
$Ile^{28}H^{\alpha}$	$Ile^{31}CH_3^{\gamma}$	450	286	484	34	$Arg^{25}H^{\alpha}$	$Ile^{28}CH_3^{\gamma}$	425	266	468	43
$Ile^{28}H^{\alpha}$	$Ile^{31}CH_3^{\delta}$	433	273	378	–	$Arg^{25}H^{\alpha}$	$Ile^{28}CH_3^{\delta}$	427	268	363	–
$Ala^{23}H^{\alpha}$	$Ala^{23}CH_3^{\beta}$	337	194	251	–	$Ser^{22}H^{\alpha}$	$Arg^{25}H_2^{\beta}$	297	243	291	–

[a] All values are given in [pm]. For determination of r^{up} and r^{low} see Experimental. For non-stereospecifically assigned CH_2 protons and for CH_3 protons r^{up} was increased by 90 and 100 pm, respectively, according to the usual pseudo-atom correction. NPY_AV_EM was generated by averaging and minimizing over the last 50 ps of the trajectory.

of 100–110 ps of the entire trajectory is shown. A close structural correspondence is found for the backbone conformation of the central residues, while the terminal dipeptide Ala^{18}-Arg^{19} and Tyr^{36} exhibit a moderately increased main-chain flexibility.

DISCUSSION

The conformational anlaysis by means of NMR of the NPY segments (18–36) and (13–36) revealed a different situation for the two molecules. While proton resonances of NPY(18–36) were quite well resolved, chemical shift values of NPY(13–36) were found to be severely overlapped. There are only little deviations within the NH resonances of corresponding amino acids (residues 18–36). The only significant difference is the extreme high-field shift of NPY(18–36) $Tyr^{21}NH$ (7.53 p.p.m.) when compared to the N-terminal extended segment NPY(13–36) ($Tyr^{21}NH$: 8.74 p.p.m.). This is in accordance to the chemical shift value of that proton observed by Mierke *et al.* [13] in hNPY under comparable conditions (Figure 10).

Comparison of the H^{α} resonances reveals that within the C-terminal portion Tyr^{20}-Tyr^{36} of both segments the H^{α} deviation $\Delta\delta_{H^{\alpha}}$ is less than 0.1 p.p.m. when compared with each other. However, the H^{α} resonances of both segments demonstrate an overall negative deviation when compared with a random sequence, thus indicating that both species adopt an α-helical conformation. In addition, the NOE patterns (Table 3) allow the formulation of a repetitive secondary structure given by an α-helix. Although in the case of NPY(13–36) it was impossible to trace an unambiguous path through the NOE pattern because of signal overlap, similar chemical shift values are typical for spins exposed to a similar chemical environment, i.e. typical for amino acids within helices. This difficulty, represented by a small range of ^1H chemical shift dispersion, often renders it necessary to apply 3D NMR techniques as demonstrated for the structure elucidation of interleukin-4 [43]. Therefore, NOE information concerning NPY(13–36) only served for a qualitative conformational evaluation, whereas the quantitative analysis of NPY(18–36) was based on numerous NMR-deduced constraints, i.e. 116 NOE- and 5 dihedral restraints. This input allowed at least a valuable description of the main-chain conformation of NPY(18–36). Thus, the results obtained by CD measurements, in addition to the qualitative NOE pattern could be confirmed by quantitative calculations by means of restrained MD. The refined conformation is in acceptable agreement with the experimentally derived parameters (Table 6). Moreover, the helical conformation is only assigned from the final structure, obtained by averaging over the last 50 ps of the trajectory, but also remains intact during the MD simulation. To illustrate this fact, selected diagnostic CO^{i}-NH^{i+4} hydrogen bonds are monitored over the trajectory in Figure 11.

Within the core region only little fluctuation of hydrogen-bond lengths are observed (Figure 11(e)–(g)), while the terminals exhibit more flexibility (Figure 11(a)–(d)). This result can be rationalized by a decreased NOE density per residue in the terminal regions when compared with the central core residues. Inspection of the χ_1 dihedral angles reveals that seven amino acids orient their side chains with a value for χ_1 of approximately 180°, two amino acids of approximately 60°, and eight amino acids of about −60° (Table 7). It should be noted that the side chain orientations as analysed by this simulation must be taken with caution, since no solvent environment was treated explicitly during the MD

Table 7 Dihedral Angles of $NPY_{(18-36)}$. All Values are Given in [°]

Residue	Torsion	NPY_AV_EM	Residue	Torsion	NPY_AV_EM
	ϕ	-		ϕ	− 63.0
	ψ	155.5		ψ	− 45.1
Ala^{18}	ω	179.6	Ile^{28}	ω	169.0
				χ_1	− 66.5
	ϕ	− 70.2		ϕ	− 61.5
	ψ	− 47.5		ψ	− 34.0
Arg^{49}	ω	177.9	Asn^{29}	ω	168.3
	χ_1	− 167.6		χ_1	− 61.4
	ϕ	− 84.8		ϕ	− 65.9
Tyr^{20}	ψ	− 24.9	Leu^{30}	ψ	− 42.1
	ω	177.8		ω	172.7
	χ_1	− 67.7		χ_1	− 168.8
	ϕ	− 66.3		ϕ	− 63.4
	ψ	− 51.0		ψ	− 48.1
Tyr^{21}	ω	173.7	Ile^{31}	ω	174.6
	χ_1	− 168.6		χ_1	− 64.2
	ϕ	− 67.1		ϕ	− 58.9
	ψ	− 40.4		ψ	− 44.6
Ser^{22}	ω	174.2	Thr^{32}	ω	177.6
	χ_1	66.9		χ_1	− 55.8
	ϕ	− 59.3		ϕ	− 75.5
Ala^{23}	ψ	− 44.6	Arg^{33}	ψ	− 50.7
	ω	172.1		ω	− 176.7
				χ_1	− 160.8
	ϕ	− 73.4		ϕ	− 75.0
	ψ	− 29.3		ψ	− 59.5
Leu^{24}	ω	167.8	Gln^{34}	ω	− 173.4
	χ_1	− 65.0		χ_1	− 173.3
	ϕ	− 65.3		ϕ	− 77.8
	ψ	− 36.9		ψ	− 55.9
Arg^{25}	ω	166.1	Arg^{35}	ω	− 176.4
	χ_1	− 167.4		χ_1	− 67.4
	ϕ	− 60.9		ϕ	− 96.7
His^{26}	ψ	− 35.1	Tyr^{36}	ψ	117.0
	ω	170.0		ω	-
	χ_1	− 68.3		χ_1	− 72.1
	ϕ	− 68.7			
Tyr^{27}	ψ	− 38.7			
	ω	167.4			
	χ_1	− 166.0			

calculations. Therefore surface artefacts, owing to over-emphasized electrostatic interactions, might have some influence.

When compared with previously published results [12–16] of structural anlayses of NPY and its analogues by 2D NMR methods, the conformation obtained for NPY(18–36) turned out to be similar within the corresponding region in terms of adopting an α-helix as expected for the C-terminal segment. While Saudek and coworkers [12, 15] described the structure of pNPY forming a dimer in aqueous solution, Darbon *et al.* [14] concluded they had a monomer under similar conditions. In contrast to the result of Saudek and coworkers, who identified intermolecular NOE correlations, Darbon *et al.* interpreted long-range NOEs as an indication for a close spatial proximity of the termini within hNPY. In this view, the structure of hNPY is characterized by

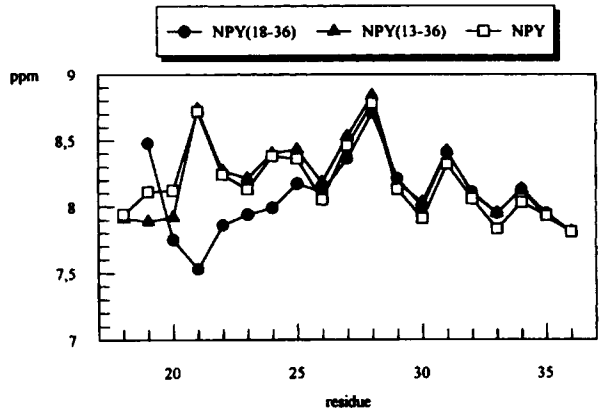

Figure 10 Comparison of the ^{1}H chemical shift values of the amide protons of residues 18–36 within the segments NPY(18–36), NPY(13–36) and the entire NPY sequence, respectively. Chemical shift values for hNPY are taken from [13].

two short contiguous α-helices comprising residues 15–26 and 28–35 which form an angle of 100°, thereby allowing an interaction between the C- and N-terminals [14]. According to Saudek and coworkers the dimer of pNPY is folded in an antiparallel manner, each monomer being composed of a largely disordered part in the N-terminal region followed by a helical segment spanning residues 11 to 36 [15]. Boulanger *et al.* [17] studied hNPY by NMR in DMSO. In contrast to the finding that the C-terminal portion adopts a more or less expanded α-helix, they did not observe an α-helix within that segment in DMSO. Under these conditions hNPY exhibits an extended structure in the N-terminal part followed by a loop including residues 10 to 17, while the C-terminal segment consists of two sections separated by a βI turn (Ile^{28}-Ile^{31}). The non-helical stretches fold around His^{26} forming an angle of 100° which is consistent with the kink of the α-helix described by Darbon *et al.* [14]. Both groups observed a proximity of the C- and N-terminal ends supporting an overall structure described by a hairpin model characteristic for the PP-fold. The conformations we obtained for both truncated analogues of NPY are characterized by an α-helix, although there is no stabilization by the N-terminal part of the NPY molecule. Boulanger *et al.* [17] proposed a disordered conformation for the corresponding portion of the molecule. The difference between the conformations we found and those cited above might be due to different solvents. However, the structures of the segments we studied show a

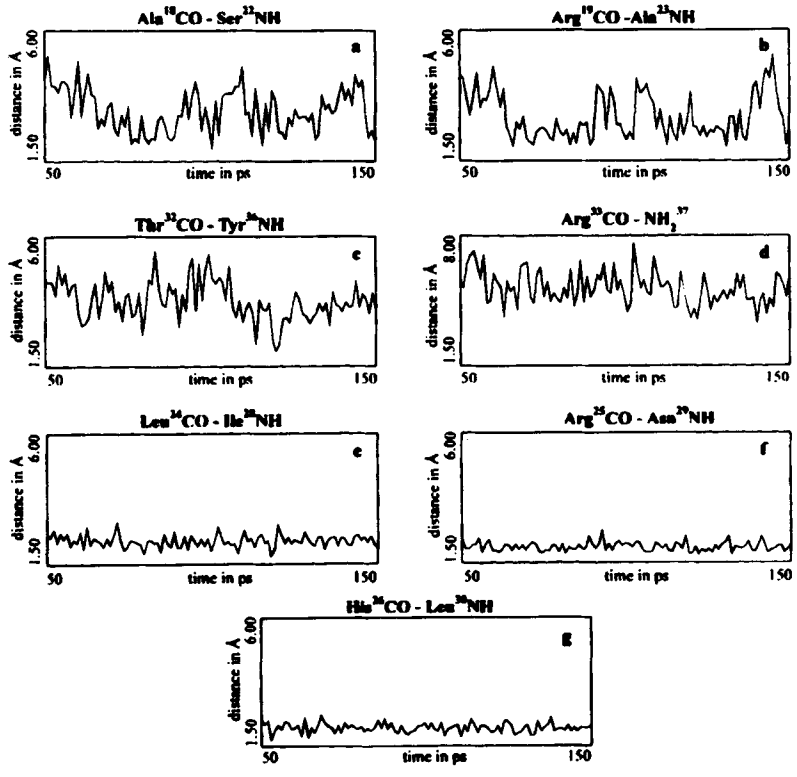

Figure 11. Behaviour of selected, diagnostic CO^i-NH^{i+4} distances of NPY(18–36) monitored over the last 100 ps of the trajectory.

striking similarity to the conformation of the C-terminal portion of the hNPY observed by Mierke *et al.* [13] in the same solvent.

Barden *et al.* [16] and Mierke *et al.* [13] studied *N*-acetyl[Leu^{28}, Leu^{31}]NPY(24–36) and hNPY, respectively, using a TFE/H_2O mixture as solvent for the conformational analysis. While the biologically active tridecapeptide mutant folded into a slightly constricted helix comprising residues 24–29, the dominating structural feature of hNPY was characterized as an α-helix in the C-terminal part extending over residues 19–34, whereas for the N-terminal portion of the molecule no regular structure was observed. With regard to these studies, which were carried out in the same solvent mixture and at the same temperature, our results are in accordance to the observation of Mierke *et al.* [13] as far as the starting residue (Arg^{19}) of the α-helix is concerned. However, the NOEs in the C-terminal region are indicative of a somewhat extended α-helical fold in this direction, at least up to Arg^{35}.

The conformations of NPY(13–36) and NPY(18–36) obtained by NMR investigations and structural refinement by molecular modelling techniques are in agreement with the conformational prerequisites proposed by structure-activity relationship studies for biologically active compounds towards NPY receptors [44, 45]. Compared with native NPY, C-terminal segments are known to exhibit only a slightly reduced affinity to the Y_2 receptor subtype compared with NPY, while the Y_1 receptor requires the entire NPY molecule [46]. From a conformational point of view the Y_1 receptor requires, first, the N-terminus associated to the C-terminus, and second, the C-terminal tetrapeptide adopting a turn-like structure [45]. In contrast, Y_2 receptor affinity is reported to involve direct interactions of the receptor with the side chains of the C-terminal dipeptide Arg^{35}-Tyr^{36}, and to require an α-helical conformation of the C-terminal NPY part [47]. The C-terminal segments (13–36) and (18–36) described above maintain the secondary structural element of the corresponding segments in the whole NPY molecule. Although there are no helix-stabilizing features from the N-terminus within these truncated NPY segments, nevertheless they adopt an extended α-helical conformation. In the structurally refined conformation of NPY(18–36) (Figure 8), the C-terminal dipeptide exposes its side chains in such a way that they are accessible to possible interaction with the receptor. To summarize, the α-helical conformation, as well as the exposure of the critical C-terminal dipeptide, allow us to rationalize the selective interaction of the segments with the Y_2 receptor subtype.

GENERAL CONSIDERATIONS

The conformations of NPY(18–36) and NPY(13–36) have been examined in 90% TFE by NMR spectroscopy. For NPY(13–36) only a qualitative conformational analysis based on CD measurements and the qualitatively interpreted NOE pattern could be performed, indicating that a significant portion of the residues adopt a helical conformation, while the structure of NPY(18–36) could be analysed in a quantitative way. The NMR-derived conformation which was refined by molecular mechanics simulations is characterized by a well-defined α-helical stretch comprising residues Arg^{19} to Arg^{35}. Comparative studies including previously published structure–activity relationships on NPY and analogues, together with our findings, allow us to derive a consistent view on receptor subtype specificities in terms of the secondary structure elements and side-chain accessibility that occur.

Acknowledgements

M. Gurrath and A. Bisello were recipients of a research fellowship from Glaxo SpA. The interest and support of Glaxo SpA. is gratefully acknowledged. We thank Dr M. Hamdan, Glaxo Research Laboratory of Verona, for mass spectrometry characterizations of all peptides studied in the present work.

REFERENCES

1. K. Tatemoto, M. Carlquist and V. Mutt (1982). Neuropeptide Y. A novel brain peptide with structural similarities to peptide YY and pancreatic polypeptide. *Nature 296*, 659–660.
2. J. C. Martel, S. St-Pierre and R. Quirion (1986). Neuropeptide Y receptors in rat brain: autoradiographic localization. *Peptides 7*, 55–60.
3. R. S. L. Chang, V. C. Lotti and T. -B. Chen (1988). Specific [^{3}H]propionyl-neuropeptide Y (NPY) binding in rabbit aortic membranes: comparisons with binding in rat brain and biological responses in rat vas deferens. *Biochem. Biophys. Res. Commun. 151*, 1213–1219.
4. J. M. Lundberg and K. Tatemoto (1982). Pancreatic polypeptide family (APP, BPP, NPY and PYY) in relation to sympathetic vasoconstriction resistant to α-adrenoceptor blockade. *Acta Physiol. Scand. 116*, 393–402.
5. J. M. Allen and S. R. Bloom (1986). Neuropeptide Y: a putative neurotransmitter. *Neurochem. Int. 8*, 1–8.

6. T. L. Blundell, J. E. Pitts, I. J. Tickle, S. P. Wood and C. -W. Wu (1981). X-ray analsis (1.4 Å resolution) of avian pancreatic polypeptide: Small globular protein hormone. *Proc. Natl. Acad. Sci. USA 78*, 4175–4179.
7. I. Glover, I. Haneef, J. Pitts, S. Wood, D. Moss, I. Tickle and T. Blundell (1983). Conformational flexibility in a small globular hormone: X-ray analysis of avian pancreatic polypeptide at 0.98 Å resolution. *Biopolymers 22*, 293–304.
8. A. D. MacKerell, Jr (1988). Molecular modeling and dynamics of neuropeptide Y. *J. Comput. -Aided Mol. Des. 2*, 55–63.
9. A. D. MacKerell, Jr. (1991). Molecular modeling and dynamics of biologically active peptides: Application to neuropeptide Y. *Methods Enzymol. 202*, 449–470.
10. V. Renugopalakrishnan, S. G. Huang, M. Prabhakaran and A. Balasubramaniam in *Peptides 1989: Proceedings of the 11th American Peptide Symposium*, J. E. Rivier and G. R. Marshall, Eds., p. 314–316, ESCOM, Leiden 1990.
11. A. Balasubramaniam, S.-G. Huang, S. Sheriff, M. Prabhakaran and V. Renugopalakrishnan in: *Proteins, Structure, Dynamics and Design*, V. Renugopalakrishnan, P. R. Carey, I. C. P. Smith, S. G. Huang and A. C. Storer, Eds., p. 79–81, ESCOM, Leiden 1990.
12. V. Saudek and J. T. Pelton (1990). Sequence-specific proton NMR assignment and secondary structure of neuropeptide Y in acqueous solution. *Biochemistry 29*, 4509–4515.
13. D. F. Mierke, H. Dürr, H. Kessler and G. Jung (1992). Neuropeptide Y: Optimized solid-phase synthesis and conformational analysis in trifluoroethanol. *Eur. J. Biochem. 206*, 39–48.
14. H. Darbon, J.-M. Bernassau, C. Deleuze, J. Chenu, A. Roussel and C. Cambillau (1992). Solution conformation of human neuropeptide Y by proton nuclear magnetic resonance and restrained molecular dynamics. *Eur. J. Biochem. 209*, 765–771.
15. D. J. Cowley, J. M. Hoflack, J. T. Pelton and V. Saudek (1992). Structure of neuropeptide Y dimer in solution. *Eur. J. Biochem. 205*, 1099–1106.
16. J. A. Barden, R. M. Cuthbertson, E. K. Potter, L. A. Selbie and A. Tseng (1994). Stabilized structure of the presynaptic (Y_2) receptor-specific neuropeptide Y analog *N*-acetyl[Leu-28, Leu-31]NPY(24–36). *Biochim. Biophys. Acta 1206*, 191–196.
17. Y. Boulanger, Y. Chen, F. Commodari, L. Senécal, A. -M. Laberge, A. Fournier and S. St-Pierre (1995). Structural characterization of neuropeptide tyrosine (NPY) and its agonist analog [Ahx^{5-17}]NPY by NMR and molecular modeling. *Int. J. Peptide Protein Res. 45*, 86–95.
18. J. Boublik, N. Scott, J. Taulane, M. Goodman, M. Brown and J. Rivier (1989). Neuropeptide Y and neuropeptide Y_{18-36}: Structural and biological characterization. *Int. J. Peptide Protein Res. 33*, 11–15.
19. A. Balasubramaniam and S. Sheriff (1990). Neuropeptide Y (18–36) is a competitive antagonist of neuropeptide Y in rat cardiac ventricular membranes. *J. Biol. Chem. 265*, 14724–14727.
20. M. W. Walker and R. J. Miller (1988). ^{125}I-Neuropeptide Y and ^{125}I-peptide YY bind to multiple receptor sites in rat brain. *Mol. Pharmacol. 34*, 779–792.
21. J. L. Krstenansky, T. J. Owen, S. H. Buck, K. A. Hagaman and L. R. McLean (1989). Centrally truncated and stabilized porcine neuropeptide Y analogs: design, synthesis, and mouse brain receptor binding. *Proc. Natl. Acad. Sci. USA 86*, 4377–4381.
22. D. R. Gehlert, S. L. Gackenheimer and D. A. Schober (1992). [Leu^{31}-Pro^{34}]neuropeptide Y identifies a subtype of ^{125}I-labeled peptide YY binding sites in the rat brain. *Neurochem. Int. 21*, 45–67.
23. M. Rance, O. W. Sorensen, G. Bodenhausen, G. Wagner, R. R. Ernst and K. Wüthrich (1983). Improved spectral resolution in COSY proton NMR spectra of proteins via double quantum filtering. *Biochem. Biophys. Res. Commun. 117*, 479–485.
24. A. Bax and G. D. Davis (1985). Practical aspects of two-dimensional transverse NOE spectroscopy. *J. Magn. Reson. 65*, 355–360.
25. G. Bodenhausen, H. Kogler and R. R. Ernst (1984). Selection of coherence-transfer pathways in NMR pulse experiments. *J. Magn. Reson. 58*, 370–388.
26. L. Müller (1987). P.E.COSY, a simple alternative to E.COSY. *J. Magn. Reson. 72*, 191–196.
27. L. Müller (1979). Sensitivity enhanced detection of weak nuclei using heteronuclear multiple quantum coherence. *J. Am. Chem. Soc. 101*, 4481–4484.
28. A. Bas and S. Subramanian (1986). Sensitivity enhanced two-dimensional heteronuclear shift correlation NMR spectroscopy. *J. Magn. Reson. 67*, 565–568.
29. G. Bodenhausen and D. J. Ruben (1980). Natural abundance nitrogen-15 NMR by enhanced heteronuclear spectroscopy. *Chem. Phys. Lett. 69*, 185–189.
30. G. Otting and K. Wüthrich (1988). Efficient purging scheme for proton-detected heteronuclear two-dimensional NMR. *J. Magn. Reson. 76*, 569–574.
31. G. Drobny, A. Pines, S. Sinton, D. Weitekamp and D. Wemmer (1979). Fourier transform multiple quantum nuclear magnetic resonance. *Symp. Faraday Soc. 13*, 49–55.
32. G. Bodenhausen, R. L. Vold and R. R. Vold (1980). Multiple quantum spin-echo spectroscopy. *J. Magn. Reson. 37*, 93–106.
33. A. J. Shaka, C. J. Lee and A. Pines (1988). Iterative schemes for bilinear operators; application to spin decoupling. *J. Magn. Reson. 77*, 274–293.
34. C. Griesinger, G. Otting, K. Wüthrich and R. R. Ernst (1988). Clean TOCSY for proton spin system identification in macromolecules. *J. Am. Chem. Soc. 110*, 7870–7872.
35. S. Macura, Y. Huang, D. Suter and R. R. Ernst (1980). Two-dimensional chemical exchange and cross-relaxa-

tion spectroscopy of coupled nuclear spins. *J. Magn. Reson. 43*, 259–281.

36. A. J. Shaka, P. B. Barker and R. Freeman (1985). Computer-optimized decoupling scheme for wideband application and low-level operations. *J. Magn. Reson. 64*, 547–552.
37. P. Daubner-Osguthorpe, V. A. Roberts, D. J. Osguthorpe, J. Wolff, M. Genest and A. T. Hagler (1988). Structure and energetics of ligand binding to proteins: *Escherichia coli* dihydrofolate reductase-trimethoprim, a drug-receptor system. *Proteins Struct. Func. 4*, 31–47.
38. K. Wüthrich: *NMR of Proteins and Nucleic Acids*, Wiley, New York 1986.
39. A. Pastore and J. Saudek (1990). The relationship between chemical shift and secondary structure in proteins. *J. Magn. Reson. 90*, 65–176.
40. K. G. R. Pachler (1963). Nuclear magnetic resonance study of some α-amino acids–I. Coupling constants in alkaline and acidic medium. *Spectrochim Acta 19*, 2085–2092.
41. B. A. Borgias, M. Gochin, D. J. Kehrwood and T. L. James (1990). Relaxation matrix analysis of 2D NMR data. *Prog. Nucl. Magn. Reson. Spectrosc. 22*, 83–100.
42. J. S. Richardson (1981). The anatomy and taxonomy of protein structure. *Adv. Protein Chem. 34*, 167–339.
43. D. S. Garrett, R. P. Powers, C. J. March, E. A. Frieden, G. M. Clore and A. M. Gronenborn (1992). Determination of the secondary structure and folding topology of human Interleukin-4 using three-dimensional heteronuclear magnetic resonance spectroscopy. *Biochemistry 31*, 4347–4353.
44. A. Beck, G. Jung, W. Gaida, H. Köppen, R. Lang and G. Schnorrenberg (1989). Highly potent and small neuropeptide Y agonist obtained by linking NPY 1–4 via spacer to α-helical NPY 25–36. *FEBS Lett. 244*, 119–122.
45. A. G. Beck-Sickinger and G. Jung (1995). Structure–activity relationships of neuropeptide Y analogues with respect to Y_1 and Y_2 receptors. *Biopolym. (Peptide Sci.) 37*, 123–142.
46. C. Wahlestedt, N. Yanaihara and R. Håkanson (1986). Evidence for different pre- and post-junctional receptors for neuropeptide Y and related peptides. *Reg. Peptide 13*, 307–318.
47. A. G. Beck-Sickinger, G. Jung, W. Gaida, H. Köppen, G. Schnorrenberg and R. Lang (1990). Structure/activity relationships of C-terminal neuropeptide Y peptide segments and analogues composed of sequence 1–4 linked to 25–36. *Eur. J. Biochem. 194*, 449–456.